The Effect of Surface Roughness on Aerodynamic Forces and Vibrations for a Circular Cylinder in the Critical Reynolds Number Range

Wenyong Ma[a,b], Qingkuan Liu[a,b], J.H.G Macdonald[c], Xudong Yan[b], Yunfei Zheng[b]

[a]Innovation Center for Wind Engineering and Wind Energy Technology of Hebei Province, Hebei 050043, China

[b]School of Civil Engineering, Shijiazhuang Tiedao University, Hebei 050043, China

[c]Department of Civil Engineering, University of Bristol, BS8 ITR, UK

Abstract: The excitation mechanism of vibrations of circular cylinders in the critical Reynolds number range remains unclear. These vibrations have been observed in wind tunnels many times but rarely in the field. The surface roughness of the cylinder might be a reason for this difference. Aiming to reveal the effect of surface roughness on the aerodynamic forces and vibrations in the critical Reynolds number range, seven circular cylinders with various value of surface roughness were covered with abrasive papers and tested in stationary and elastically mounted wind tunnel tests. The results show that the surface roughness significantly influences the aerodynamic forces in the critical Reynolds number range by reducing the range of transitions on boundary layers. These influences include suppressing the jumps in lift coefficients and other phenomena that relate to a bistable state occurring only for less rough cylinders. Therefore, sufficient surface roughness can mitigate the vibrations in the critical Reynolds number range by suppressing the bistable state in which the vibrations appear.

Keywords: Circular cylinder; Critical Reynolds number; Surface roughness; Aerodynamic forces; Large amplitude vibration.

1. Introduction

Dry galloping has attracted much interest for several years and has been reproduced in wind tunnel tests(Cheng et al, 2008a; Cheng et al, 2008b; Jakobsen et al, 2012; Ma et al, 2017b; Ma et al, 2017c; Nikitas et al, 2012;Nikitas and Macdonald, 2015). Even though the mechanism for these vibrations remains unclear, the critical Reynolds number plays an important role in their behaviour(Cheng et al, 2008b; Matsumoto et al, 2010; Matteoni and Georgakis, 2015; Nikitas and Macdonald, 2015). Therefore, the surface roughness is expected to have a significant influence on these vibrations in the critical Reynolds number range because of the sensitivity of the flow state to surface conditions in this regime.

The critical Reynold number range was first used to describe the flow state corresponding to the drag crisis in the plot of drag coefficient against Reynolds number. In this range, a transition occurs close to or in the boundary layers on the surface of the circular cylinder. The flow state in the critical Reynolds number range can be divided into three specific regimes, pre-critical (TrBL0), one separation bubble (TrBL1) and two separation bubbles (TrBL2) (Zdravkovich, 1997a). Eisner (1925) first discovered an asymmetric pressure distribution for a limited time in the TrBL1 regime. It took several decades to confirm this phenomenon because an asymmetric average pressure distribution on a circular cylinder in symmetric flow was not expected. Bearman (1969) found discontinuous changes in the base pressure coefficient and vortex shedding frequency with increasing Reynolds number in the critical range. He also found that the separation bubble formed consistently on the same side without obvious asymmetries in either the tunnel flow or the model geometry in TrBL1 regime. Schewe (1983) also found that the single separation bubble in the TrBL1 regime, once formed, can be stable. Furthermore he showed that there is no preference for one side, thus the state of the flow is bistable. He also demonstated that the flow can be tripped by very small perturbations from TrBL0 to TrBL1 with the bubble on either side (Schewe, 1986). Hence, it is hard to predict the asymmetric states and the sign of the steady lift for a circular cylinder. The characteristics of aerodynamic forces in these three regimes depend on the flow transition on the boundary layer which is very thin at high Reynolds numbers. The effect of surface roughness on transition in the boundary layer can be understood from two aspects. First, surface roughness influences the formation of the boundary layer by increasing the skin friction. Therefore, the boundary layer grows more quickly on rougher surfaces. When the irregularities protrude through the boundary layer, the flow state will differ from that when the irregularities are wholly embedded within the boundary layer. Second, a rough surface induces turbulence at a similar scale to the thickness of the boundary layer. The roughness-generated turbulence may have a significant influence on the transition.

Both aspects are strongly related to the transition process in the boundary layer. Therefore, surface roughness significantly influences all aspects of the characteristics of aerodynamic forces in the critical Reynolds number range. In general, surface roughness causes the drag crisis to occur at a lower Reynolds number, reduces the critical Reynolds number range and weakens the drop in the drag coefficient. Moreover, surface roughness can induce roughness-generated turbulence which influences the formation of the boundary layer and the occurrence of the transition. The TrBL0, TrBL1 and TrBL2 regimes found for the smooth cylinder are disturbed by the slight surface roughness. For high surface roughness, TrBL1 and TrBL2 are eliminated(Zdravkovich, 1997b).

The large amplitude vibrations of the circular cylinders in the critical Reynolds number range have been explained in term of three main aspects: unsteadiness of the flow state (Nikitas and Macdonald, 2015), imperfections of the circular cylinder(Benidir et al, 2015; Matteoni and Georgakis, 2015), and axial flow for inclined cylinders(Matsumoto et al, 2010). Large amplitude vibrations in the critical Reynolds number range for a smooth elliptical cylinder under normal wind have also been observed in wind tunnel tests(Ma et al, 2017b; Ma et al, 2017c). The results imply that imperfections and axial flow may not be necessary conditions for vibrations in the critical Reynolds number range. Therefore, dry galloping is more likely to depend on the unsteady flow in the critical Reynolds number range. In this range, the flow state and characteristics of aerodynamic force vary across the three regimes, TrBL0, TrBL1, and TrBL2. Compared with the mean drag coefficient, the lift coefficient experiences even more significant variation in the mean and fluctuation components. The jumps in lift coefficients(Benidir et al, 2015; Jakobsen et al, 2012; Ma et al, 2017c; Nikitas and Macdonald, 2015) represent a transition process between the TrBL0 and TrBL1 regimes. The non-zero mean lift coefficient is induced by a separation bubble on one side of the cylinder in the TrBL1 regime. The narrow wake produced by the reattachment also creates a weak component in the fluctuation of lift that is related to vortex shedding. Energy concentrated at low frequencies (much smaller than the frequency of vortex shedding) is contributed by the pressures in the separation bubble region. All the above variations in lift influence the vibrations in the critical Reynolds number range and are affected by the surface roughness. However, the flow regime in which dry galloping occurs and the effect of surface roughness on them remains unclear. From the practical point of view, dry galloping has been observed in wind tunnel tests many times, and they have been reproduced by the author's group for circular cylinders under normal and skew winds(MA et al, 2017a; Ma et al, 2017b; Ma et al, 2017c). However, these vibrations are rarely observed in the field. Turbulence and surface roughness might be two significant factors to explain the differences in behaviours in wind tunnel tests and field observations. Considering that the turbulence integral scale of the wind in the field is much larger than the scale of the boundary layer on the surface of the circular cylinder, the effect of surface roughness is more likely to correspond to this difference and should be studied first(Zdravkovich, 1997b).

This paper aims to reveal the effect of uniform surface roughness on the aerodynamic forces and vibrations of circular cylinders in the critical Reynolds number range and to clarify the flow regimes in which the large amplitude vibrations occur. The surface roughness was simulated by covering the cylinder with silicon carbide abrasive paper. Seven models with various values of surface roughness were tested for static aerodynamic forces with high-frequency balances at both ends and for across-wind vibrations through a single-degree-of-freedom elastically mounted system.

2. Experimental setup

The static and dynamic tests were carried out in the wind tunnel at Shijiazhuang Tiedao University, which has a working section 2.2 m wide and 2 m high. The turbulence intensity in the working section is approximately 0.2% at a wind speed of 63 m/s and less than 0.6% when wind speed is larger than 15m/s. Seven models with different surface roughnesses were tested in static and dynamic tests. The smooth model was made of plexiglass, and the six others were covered by abrasive papers.

The models were 1.7 m in length, L. The diameters at 20 random locations of each model were averaged to obtain the diameter of each model, D. As listed in Table 1, the difference in the diameters between the model was less than 1mm. D=120 mm, corresponding to a blockage ratio of 6%, was used to estimate the Reynolds numbers, force coefficients, and normalized displacements. The abrasive papers were termed P5000, P3000, P1200, P600, P100, and P60, respectively, as shown in Table

1. These numbers such as P5000 indicates the number of grits in each square centimeter. The larger the number is, the smaller the grits are and the finer the paper is. In the present study, the surface roughnesses were quantified by four parameters, P_a, P_z, K and K/D. K is the nominal equivalent diameter of the sand or grit on the abrasive paper, which is provided by the manufacturer. P_a and P_z are the average protrusion height and mean square value of the protrusion height of the abrasive paper, respectively, which were measured by putting the paper on a horizontal stand before covering it on the cylinder (Mitutoyo SJ-410). K/D is the normalized surface roughness, which was selected to describe the models in the present study because it was widely used in the previous studies(Zdravkovich, 1997b).

To reduce the influence of free ends, the compensation models and end plates were used together in the static tests, as shown in Fig. 1. Two high-frequency balances (ATI Delta), were mounted at the ends of the cylinder and covered by compensation models that were tubes with the same diameter as the model. The high-frequency balances were rigidly supported by the outside braces in static tests. The stiffness of models was provided by a steel tube inside of the cylinder which provided the bending frequencies from 17Hz to 20Hz. The circular end plates with a diameter of D_e=720 mm were mounted at the end of the compensation models less than 1 mm away from the test model.

The same models were used in the dynamic tests, but the compensation models and high-frequency balances were removed, and end plates were mounted at the ends of the cylinder. To reproduce a single-degree-of-freedom system, four springs were vertically mounted at each end of the cylinder through a horizontal end bar outside the wind tunnel, as shown in Fig. 1 (b), and horizontal motions were restricted by connecting the end of the cylinder to a stationary point through a 6 m long wire at each end. Two force metres were mounted at the end of the lower springs. The displacements were estimated through the measured the forces and the stiffness of the springs. The setup provided the natural frequencies, f_v=2.44-2.47 Hz and damping ratios, ζ=0.09%-0.17%, as shown in Table 1.

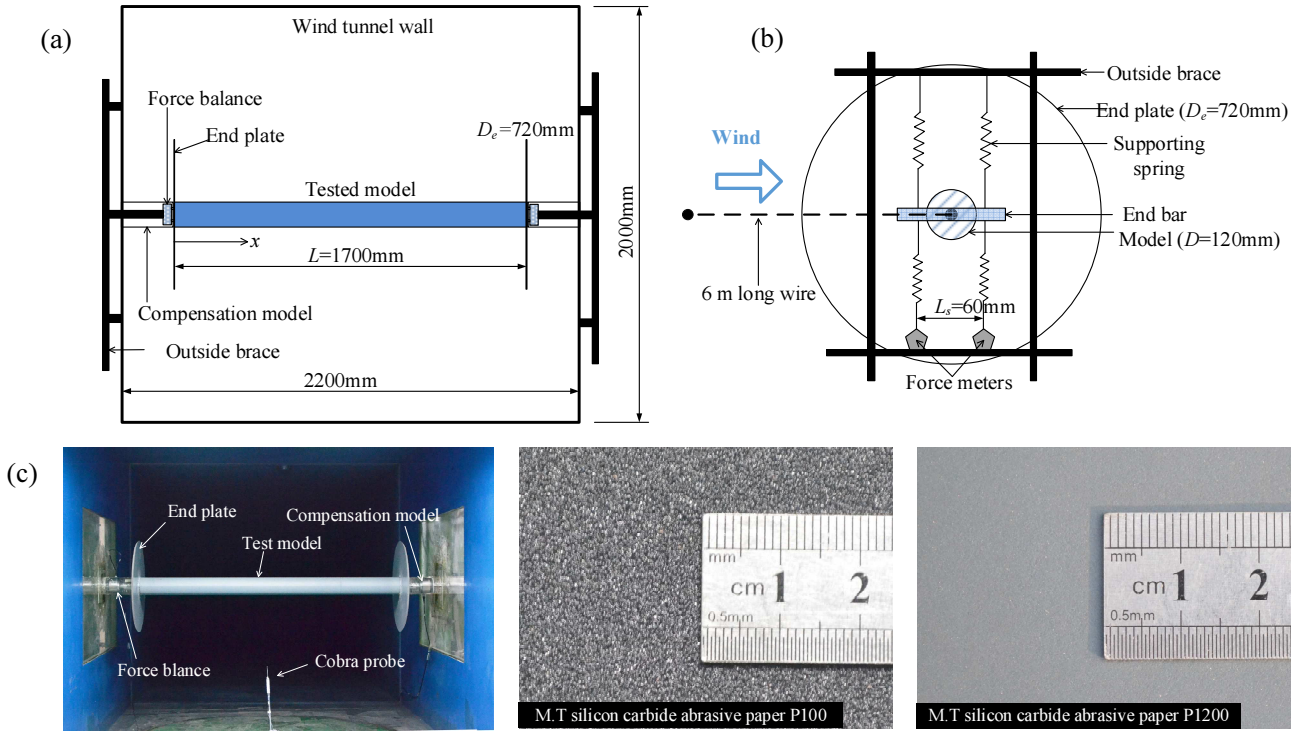

Fig. 1 Schematics of the wind tunnel arrangement and the model with the main parameters indicated: (a) the model and end conditions, (b) the support system at the end in dynamic tests and (c) the model in the wind tunnel and abrasive papers.

Table 1 Shape parameters, dynamic parameters and Reynolds numbers for the different models

	Plexiglass	Abrasive paper covered					
	Smooth	P5000	P3000	P1200	P600	P100	P60
D(mm)	120.13	120.39	120.40	120.56	120.43	120.60	120.98

P_a(μm)	0.52	5.36	5.84	5.98	11.24	41.06	75.02
P_z(μm)	2.01	26.52	29.92	34.73	56.66	207.51	349.73
K(μm)		2.6	6	11	23	150	250
K/D		0.002%	0.005%	0.009%	0.019%	0.125%	0.208%
f_v(Hz)	2.47	2.47	2.47	2.47	2.46	2.46	2.44
ζ	0.15%	0.17%	0.09%	0.11%	0.11%	0.11%	0.11%
Re (10^5) for static tests	1.21-4.33	0.57-4.61	0.56-4.63	0.56-4.63	0.56-4.62	0.56-3.89	0.56-4.04
Re (10^5) for dynamic tests	1.24-4.23	0.83-4.21	0.81-4.23	0.81-4.21	0.81-4.24	0.51-3.51	0.50-3.58

The wind speeds were varied from approximately 6 to 55 m/s at various intervals, corresponding to the Reynolds numbers listed in Table 1. Please note that the wind speed in the present study is far away from the critical wind speed for the conventional vortex induced vibration in the subcritical Reynolds number range which is less than 1.48-2.98m/s based on St=0.2 and natural frequency approximate 2.47Hz. All the ranges of Reynolds number were aimed to cover the "drag crisis" regime to ensure the characteristics of the aerodynamic forces and to ensure that the related vibration in the critical Reynolds number range could be observed. The forces measured in the static tests using the high-frequency balance were recorded at a frequency of 1500 Hz, and the forces obtained in the dynamic tests from the force metres were recorded at 500 Hz.

To illustrate the difference between the static aerodynamic forces at the two ends, mean aerodynamic force coefficients are shown in Fig. 2 (a) and (b) for the smooth cylinder and the cylinder with K/D=0.009%, respectively. In Fig. 2, the force coefficients at each end are normalized by $1\backslash 2(\rho U^2 DL)$. C_{DL}, C_{DR}, C_{LL} and C_{LR} present the mean value of drag coefficient at left, drag coefficient at right, lift coefficient at left and lift coefficient at right, respectively. It should be noted that the mean value of aerodynamic force coefficient is average of force coefficients in whole sampling period even when aerodynamic force suddenly change with time in the critical Reynolds number range. The results at both ends agree well except in the range where the large (in magnitude) mean lift coefficients occur. This difference in lift coefficients may be attributed to the three-dimensional flow in the critical Reynolds number range, in which the separation bubble may form over a certain length of the cylinder that may not be symmetrical over the total length. The sum of the aerodynamic forces at both ends is used to give the total forces on the cylinder in the present study. In Fig. 2 (c), D_{vL} and D_{vR} are the vertical displacements at the left and right end, respectively. D_t indicates the end to end rotation. A reasonable agreement between the normalized vertical displacements at both ends is shown in Fig. 2 (c) for the smooth cylinder at Re=3.73×10^5 in the dynamic tests. The maximum D_t is approximately 2^o. A similar agreement between the displacements at the two ends was found for all the tests with significant vibrations. The displacements of the cylinder are estimated by averaging the displacements measured at the two ends. To confirm the phenomena and check the consistency, the static tests were carried out three times for each model at the same conditions. The dynamic tests were also carried out two times.

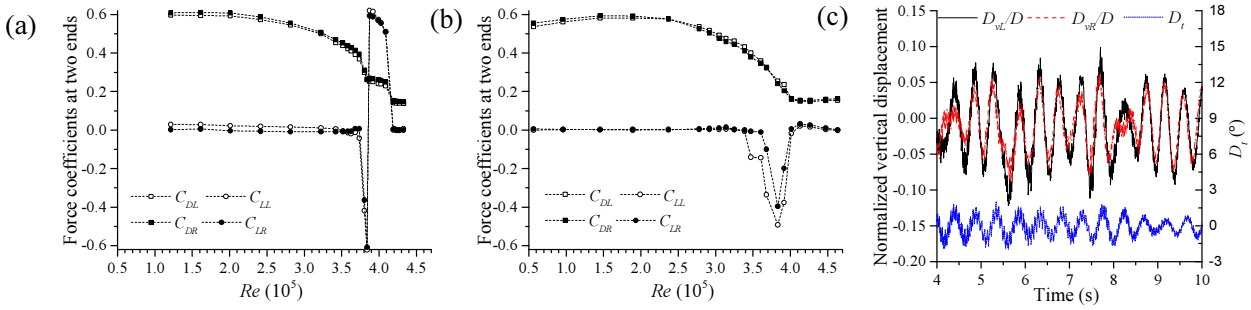

Fig. 2 The difference between the measured results at both ends for stationary tests on (a) smooth cylinder, (b) K/D=0.009%, and for dynamic tests on a (c) smooth cylinder at Re=3.73×10^5

3. Aerodynamic forces on stationary cylinders

3.1 Effects of surface roughness on drag crisis and mean aerodynamic force coefficients

The variations of mean drag and lift coefficients with Reynolds number and surface roughness for the three tests are shown in Fig. 3. A significant feature in the critical Reynolds number range is the sudden drop in the drag coefficient curve known as the 'drag crisis,' which was observed for all tested models, as shown in Fig. 3 (a). The precritical regime (TrBL0), the start of the critical state, is characterized by the first onset of flow transition in free shear layers along separation lines(Zdravkovich, 1997a). TrBL0 covers a wide Reynolds number range from the initial fall in the drag coefficient to the formation of a separation bubble in TrBL1. A separation bubble on one side creates a non-zero mean lift on the cylinder, as shown in Fig. 3 (b). With further increase in the Reynolds number, another separation bubble forms on the other side of the cylinder, which creates symmetrical flow state again and obliterates the average lift. The flow enters the TrBL2 regime. However, the one bubble regime may not occur in a high roughness surface cylinder.

In general, the trends in the variations of aerodynamic forces for the three tests agree well, but a notable difference can be observed in the variation of lift coefficients with the Reynolds number, as shown in Fig. 3 (b), (d) and (f). The direction of the mean lift in a certain range of Reynolds numbers changes with surface roughness. It is also different for the three tests. Furthermore, the direction of the mean lift coefficients also changes with the Reynolds number for the same model in one test, such as a smooth cylinder and K/D=0.002% for the first test, K/D=0.009% and 0.019% for the second test, and K/D=0.005%, 0.009% and 0.019% for the third test. These changes imply that the separation bubbles change sides and do not coincide with the early studies(Bearman, 1969; Schewe, 1983). Bearman(Bearman, 1969) wrote in 1969: 'The distribution of base pressure along the span suggested that the establishment of a bubble on one side takes place along the complete length of the cylinder and this was later confirmed by the surface oil flow pattern. There were no particularly obvious asymmetries in either tunnel flow of the model geometry to suggest that asymmetry bubbles formed consistently on one same side'. In 1983, Schewe (Schewe, 1983) believed that the formation of the separation bubble might occur on either side of the cylinder, but once established it could not change sides. Three years later, Schewe[Schewe, 1986] proved that very small perturbations on the surface of a circular cylinder significantly change the flow state around the cylinder, which means it is very hard to make a sufficient symmetric model in the TrBL0 regime, especially over the entire length of the cylinder. Therefore, the change in the direction of lift coefficients is more likely to be a widely encountered feature in one bubble regime for a finite length imperfection circular cylinder.

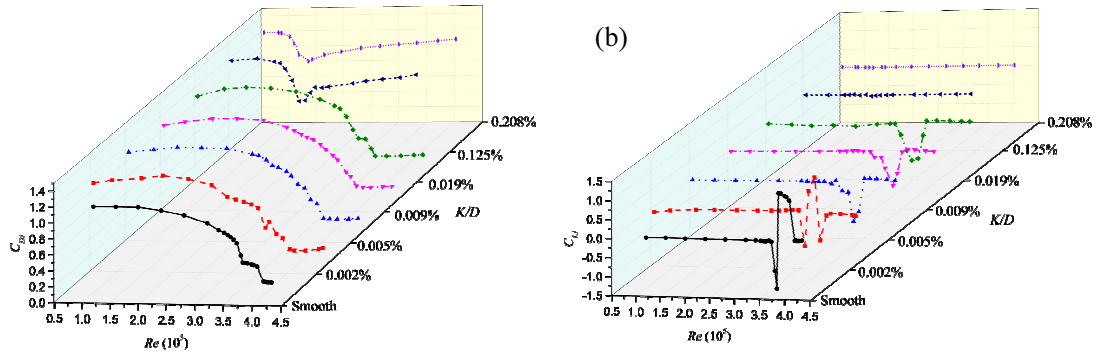

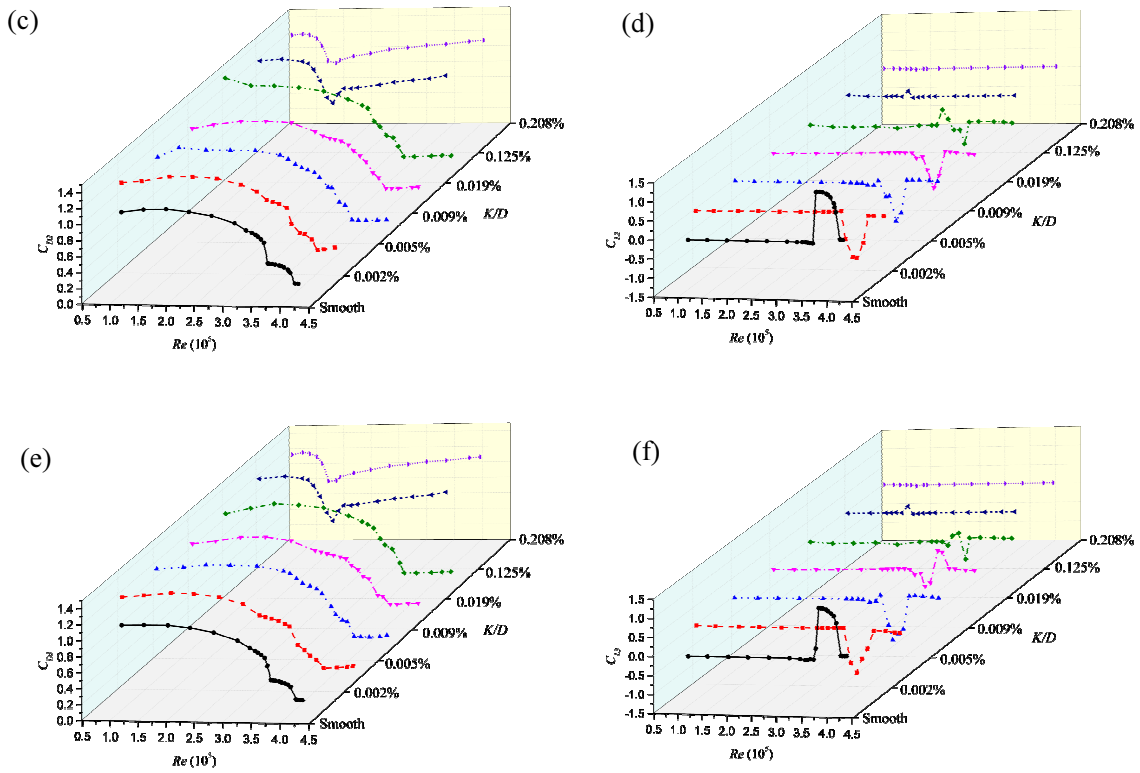

Fig. 3 Mean force coefficients in terms of *Re* for various roughnesses (a) C_{D1} (b) C_{L1} (c) C_{D2} (d) C_{L2} (e) C_{D3} and (f) C_{L3}.

The minimum drag coefficient C_{Dmin}, which designates the end of TrBL2 or the start of TrBL3, and the corresponding Reynolds number are used to illustrate in Fig. 4 the effect of surface roughness on the occurrence of the drag crisis. The maxima of the absolute value of the mean lift coefficient $|C_L|_{\max}$ and the corresponding Reynolds number are also shown in Fig. 4. To reduce the random influence in the tests, the results of three separate tests termed for each cylinder are included in Fig. 4. Achenbach's results (Achenbach, 1971, 1981) are also shown in Fig. 4 for comparison.

Fig. 4 (a) shows good agreement in C_{Dmin} between the three tests with the different surface roughnesses, distinguished by subscripts 1, 2 and 3. The trends in C_{Dmin} indicate a wider wake for the cylinder with a smoother surface. It also implies the final separation point moves upstream as the surface becomes rougher. The values of $|C_L|_{\max}$ indicate the strength of the separation bubble. The trends in $|C_L|_{\max}$ show a significant reduction with increasing surface roughness. For the cylinder with the roughest surface, K/D=0.208%, $|C_L|_{\max}$ is nearly zero, which means that an asymmetrical wind pressure distribution disappears in this case. It also means that the TrBL1 flow state is mitigated by the sufficient transition at the rough surface.

The C_{Dmin} and $|C_L|_{\max}$ occurs at lower Reynolds numbers for cylinders with rougher surfaces, as shown in Fig. 4 (b). The transition occurs at a lower Reynolds number for the rougher model. Furthermore, the difference in the Reynolds numbers corresponding to C_{Dmin} and $|C_L|_{\max}$ becomes insignificant at K/D=0.125% and 0.208%. This indicates that the transition takes place over a narrow Reynolds number range for rough cylinders. The scatter of $|C_L|_{\max}$ and the corresponding Reynolds numbers for the three tests shown in Fig. 4 implies that the wind pressures on the two sides of the cylinders are sensitive to small disturbances.

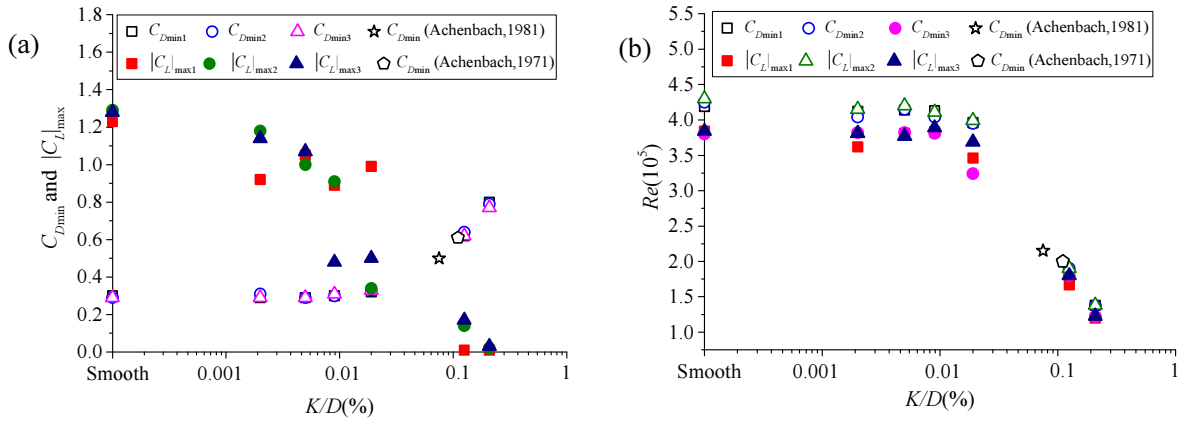

Fig. 4 Influence of roughness on (a) the minimum drag coefficient, C_{Dmin}, and the maximum lift coefficient, $|C_L|_{max}$, and (b) the corresponding Re of C_{Dmin}.

3.2 Effects of surface roughness on lift coefficient fluctuations and the Strouhal number

To identify the effects of surface roughness on lift coefficient fluctuations and the frequency of vortex shedding, first the flow regimes must be clarified. Fig. 5 shows the mean drag coefficient C_D, the Strouhal number St, the standard deviation of the lift coefficient C_{Lr} and spectra of the lift coefficient, S_{PCL} at various Reynolds numbers for the smooth circular cylinder. To identify the contribution of vortex shedding to the lift coefficient fluctuations, the lift coefficients were bandpass filtered in the normalized frequency range fD/U=0.1~0.5, because Strouhal numbers are generally in this range for the flow around circular cylinders (Zdravkovich, 1997a). Fig. 5 also shows the standard deviation of the filtered lift coefficients C_{Lrs}. In the present study, St is considered the dominant normalized frequency in the range of fD/U=0.1~0.5 in the spectrum of the lift coefficients. Therefore, St can only be identified when the vortex shedding has a discernible contribution to the lift coefficient fluctuation fluctuations.

Based on the plot of the C_D curve against the Reynolds number, Fig. 5 (a) indicates four flow regimes, namely, a transition in the shear layers TrSL3 (Re<2.0×10^5), precritical TrBL0 (Re≈2.0-3.8×10^5), one bubble TrBL1(Re≈3.8-4.1×10^5) and two bubbles TrBL2 (Re>4.1×10^5). As the Reynolds number increases, C_D remains constant in TrSL3, then gradually decreases in TrBL0, and then suddenly drops to TrBL1 and remains constant before the second drop to TrBL2. A clear plateau of the C_D curve in TrBL1 represents a stable single separation bubble on one side of the cylinder. The reduction in the drag coefficient implies a narrowing of the wake. A narrower wake tends to lead to a higher frequency of vortex shedding(Zdravkovich, 1997a). As shown in Fig. 5 (a), C_D=0.5 and St=0.31 in TrBL1, C_D=0.29 and St=0.45 in TrBL2. Fig. 5 (b) shows the standard deviation of the lift coefficient, C_{Lr}, which represents the strength of the fluctuation in the lift, and the standard deviation of the filtered lift coefficient, C_{Lrs}, which represents the strength of fluctuation in the lift caused by vortex shedding. The standard deviation of the lift coefficient decreases as the Reynolds number increases in TrSL3 and the early stage of TrBL0 and the fluctuations are primarily caused by vortex shedding, as shown in Fig. 5 (c). In the TrBL1 and TrBL2 regimes, the lift coefficient fluctuations are very weak compared to that in TrSL3, and vortex shedding contributes less to the lift coefficients. The strong fluctuations around Re=3.8×10^5 in the range of the transition from TrBL0 to TrBL1 are due to the intermittent jumps in the lift, which have been found in previous studies(Benidir et al, 2015; Ma et al, 2017c; Nikitas and Macdonald, 2015) and will be discussed in section 3.3.

In the critical Reynolds number range, the occurrence of peaks in the lift spectra at low frequencies, well below the frequency of vortex shedding and contributing much to the lift coefficient fluctuations, may be related to the transition in the boundary layer. The fluctuation in lift coefficients is primarily contributed by the fluctuating wind pressures on the sides of the cylinder. The transition probably contributed to the fluctuation when it occurred in the boundary layer. On the other hand, the transition in the boundary layer also makes a reattachment which narrows the wake and reduces

the vortex related pressure fluctuation on the sides of the cylinder. The normalized peak frequency for the low-frequency components, $f_N=fD/U$, is used to distinguish the normalized vortex shedding frequency St. Notably, f_N is approximately 0.05, which agrees well with Nikitas's results[Nikitas et al, 2012], $fD/U<0.05$, for the inclined cables. In the present study, the corresponding frequencies are approximately 15Hz to 20Hz in the critical Reynolds number range. Nikitas[Nikitas et al, 2012] believes that the low-frequency components are probably a response to vibrations of the dry inclined cables. He thinks that low-frequency forcing is probably related to wake vortex shapes for $fD/U<0.1$. However, this fails to explain why the vortex is in the low-frequency range for the narrow wake flow state. These low-frequency components are more likely related to the separation and reattachment on the side of the cylinder than to the vortex in the wake. The bending frequency of the cylinder is 17Hz to 20Hz approximately corresponding to the $0.04<fD/U<0.05$. Therefore, the peaks in the low frequency ($0.04<fD/U<0.05$) also reflect the response of the model to wind pressure distribution changing between the symmetric and asymmetric. These peaks should be considered as the combination of aerodynamic forces caused by the bistable flow state and inertial forces of the bending vibration.

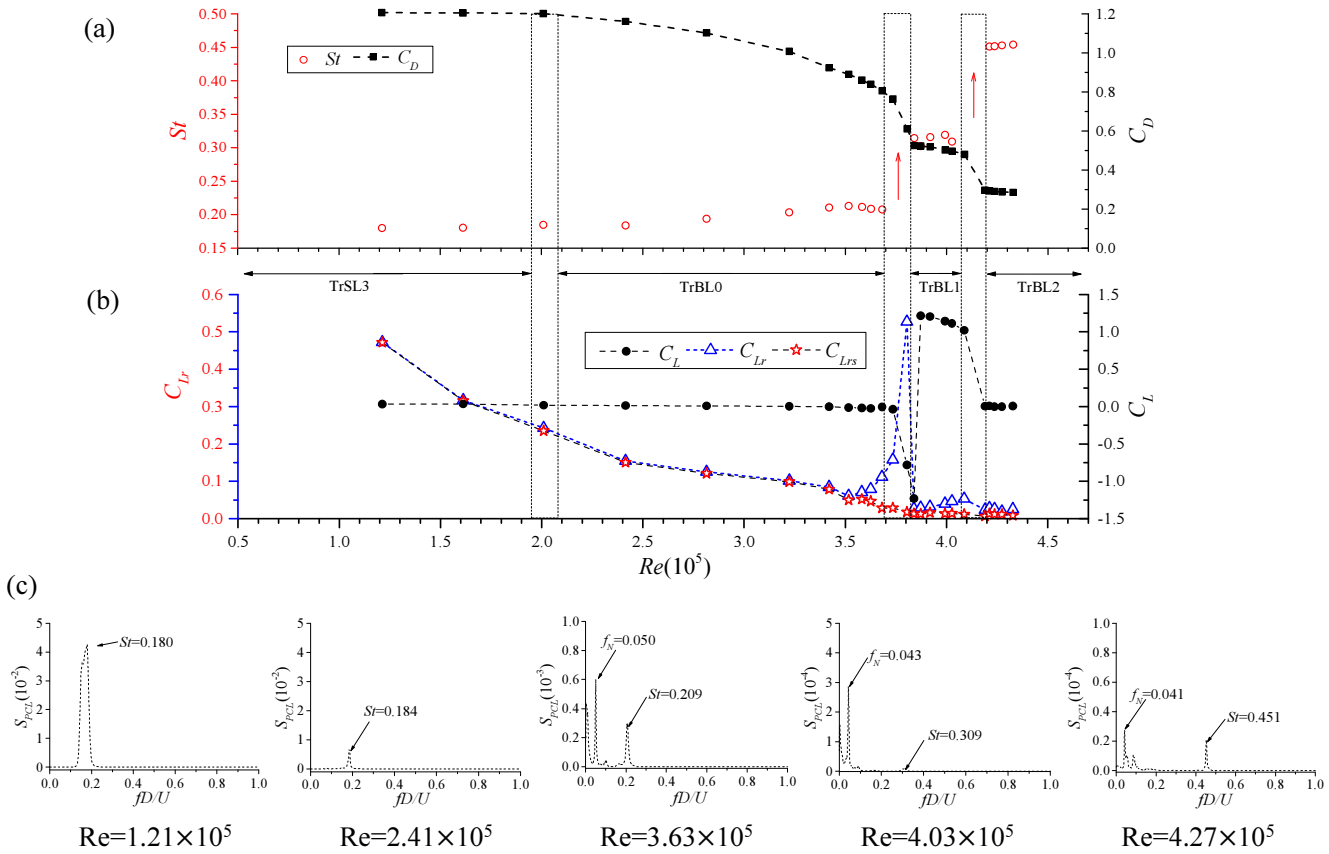

Fig. 5 Variation in characteristics of aerodynamic forces in terms of Re for (a) C_D and St (b) C_L, C_{Lr} and C_{Lrs} (c) S_{PCL}

Fig. 6 shows the variation of C_D , St , C_L, C_{Lr} and C_{Lrs} with Re for the different values of surface roughness as K/D . When the surface roughness is small, as shown in Fig. 6 (a,b,c and d), St can only be identified before the drag crisis. When K/D=0.125% (Fig. 6 (e)), St cannot be identified in only one case, at $Re=1.80\times10^5$, corresponding to the minimum C_D. When K/D=0.208% (Fig. 6 (f)), St can be identified for the entire tested Reynolds number range. The C_{Lr} and C_{Lrs} curves at low K/D show that the contribution of vortex shedding to the standard deviation of lift coefficients is very weak in the critical Reynolds number range. The differences in C_{Lr} and C_{Lrs} decrease for rougher cylinders. When K/D=0.208% (Fig. 6 (f)), the lift coefficient fluctuations are dominated by vortex shedding over the entire Reynolds number range, which in turn is dominated by the negligible difference between C_{Lr} and C_{Lrs}. Similar to the smooth cylinder, C_{Lrs} gradually decreases with increasing Reynolds number in the TrBL0~TrBL2 range for low K/D, as seen in Fig. 6 (a,b,c and d). When K/D is high, as in Fig. 6 (e and f), C_{Lrs} is higher than the values for low K/D in and beyond the TrBL2 regime. This stronger vortex shedding beyond the drag crisis range for the rougher cylinders is probably associated with the wider wake, which corresponds to the separation points being farther windward and the drag

coefficients being larger.

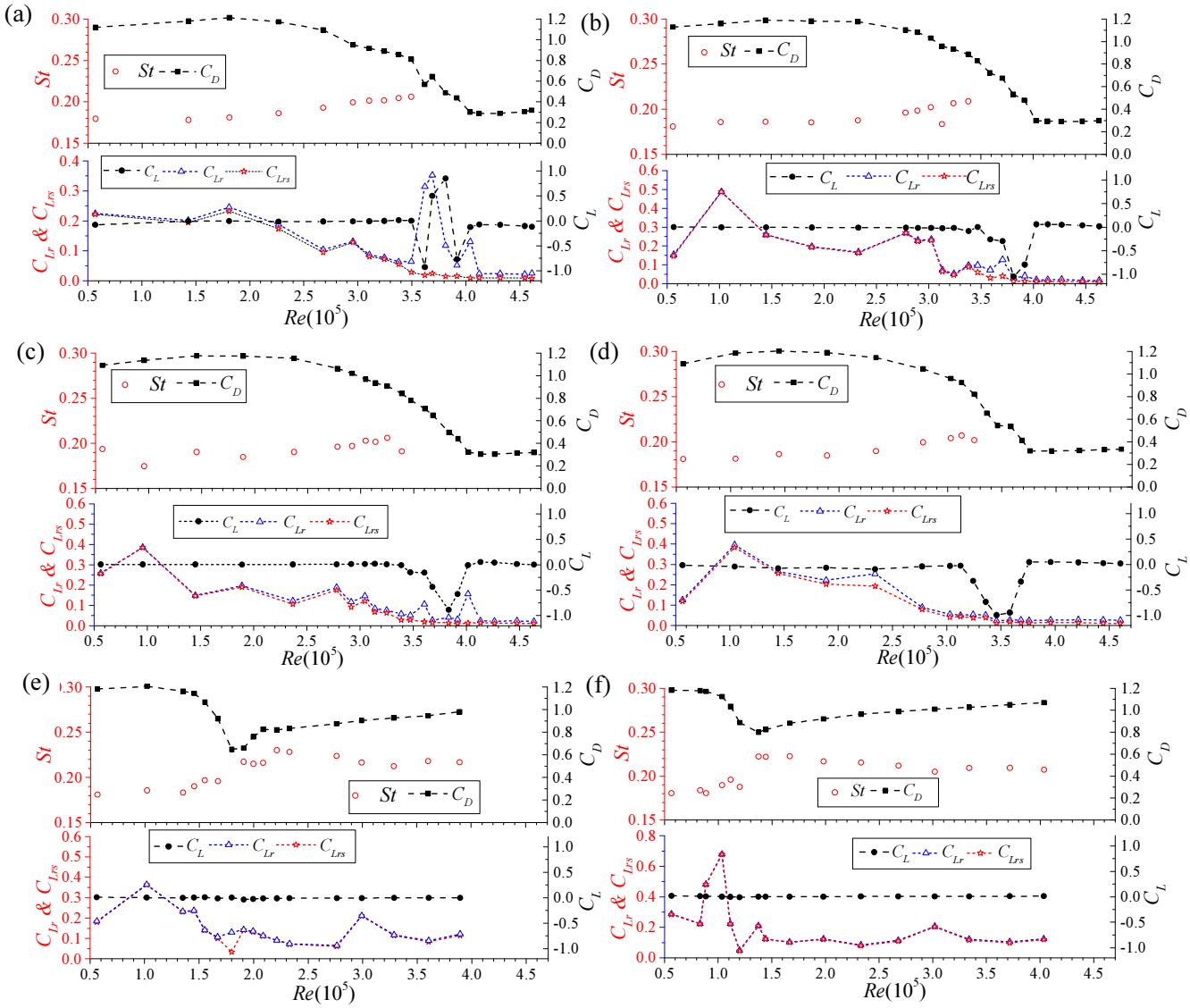

Fig. 6 Variation in C_D , St , C_L, C_{Lr} and C_{Lrs} with Re at K/D= (a) 0.002% (b) 0.005% (c) 0.009% (d) 0.019% (e) 0.125% (f) 0.208%.

To show the variation in the low-frequency components in the critical regime, the spectra of lift coefficients for three different values of surface roughness (smooth, K/D=0.019% and K/D=0.208%), are shown in Fig. 7. The Reynolds numbers in Fig. 7 are chosen to represent the flow state in the drag crisis. In contrast in subcritical range, the peaks at low frequency (fD/U<0.1) are far away from the vortex shedding frequency (fD/U≈0.31 in TrBL1 for the smooth cylinder). This implies that there are relatively strong non-vortex contributions to the fluctuations in the lift coefficients. The non-vortex contributions decrease for the rough cylinder, whereas the vortex shedding contributes more. Because the low-frequency fluctuations are probably related to the transition in the boundary layer occurring in the TrBL1 and TrBL2 regimes, the weaker low-frequency component for the rougher surface cylinder, as seen in Fig. 7 (c), could be attributed to the effect of surface roughness on the boundary layer transition. The rough surface induces turbulent flow in the boundary layer. The turbulence has a significant influence on the transition and weakens the separation bubbles. Once the rough surface protrudes through the boundary layer, the TrBL1 and TrBL2 states disappear. The flow around the cylinder moves straight from TrBL0 to TrBL3. Therefore, strong low-frequency fluctuations were not observed for K/D=0.208%.

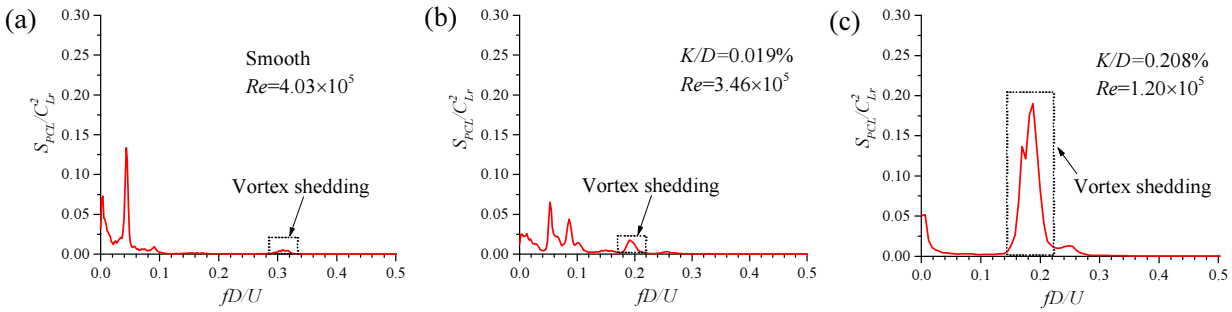

Fig. 7 Low frequency and vortex shedding components in lift coefficients at (a) smooth cylinder (b) K/D=0.019% (c) K/D=0.208%.

In the present study, the frequency of vortex shedding is identified through the spectra of lift coefficients. However, the vortex shedding may have an inconsiderable influence on the lift when it is very weak, or the wake is very narrow. Thus, the vortex shedding may not be identified when the flow separates at the rear of the cylinder. Fig. 8 shows the relationship of St to C_D for various values of surface roughness. The general trend in Fig. 8 agrees well with the common understanding that a low C_D corresponds to a narrow wake and a high St (Zdravkovich, 1997a). It also shows that, for the same C_D, surface roughness has a negligible effect on St. When C_D=1.18, St=1.84 and 1.83 for the smooth cylinder and K/D=0.208%, respectively. The Strouhal numbers for the same C_D in different flow states are also close. For K/D=0.208%, St=1.96 when C_D=1.03 in the precritical regime, and St=2.09 when C_D=1.03 in the post-critical regime.

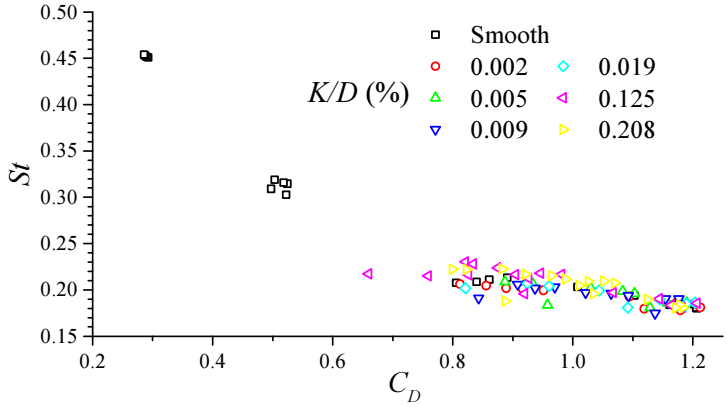

Fig. 8 Variation in St with C_D at various relative roughnesses and Reynolds numbers.

3.3 Effects of surface roughness on the fluctuation in the transition

Over the entire critical Reynolds number range, there are three flow regimes, TrBL0, TrBL1, and TrBL2. An interesting feature of jumps in the lift coefficient has been discussed for the cases of a circular cylinder(Jakobsen et al, 2012; Nikitas and Macdonald, 2015), an imperfect circular cylinder(Benidir et al, 2015) and an elliptical cylinder(Matsumoto and Ishizaki, 2017) related to the TrBL0 to TrBL1 transition, which is here termed TrBL0-1. These jumps were also observed in the present study. For example, Fig. 9 (a) corresponds to Re=3.81×10^5 in Fig. 5 (a). The jumps are only observed for the four smoothest models, and all of them are related to TrBL0-1. The occurrence of the jumps implies that at least two flow states may exist in the transition range. When there is reattachment on one side of the cylinder, a non-zero average lift coefficient appears. As shown in Fig. 4 (b), the maximum average lift coefficient decreases with increasing surface roughness. The jumps in the lift coefficients also become weaker for the rougher cylinders. As shown in Fig. 9, the lift coefficients jump from zero to -1.2 for the smooth cylinder, and from zero to -0.5 for K/D=0.009%. Finally, these jumps disappear for K/D=0.019% or greater. From our observations of all the tests, the jumps occur in a small Reynolds number range, corresponding to TrBL0-1, which becomes narrower for rougher surfaces because roughness improves the efficiency of the transition. In the present study, when K/D=0.208%, the TrBL 1 regime was not observed.

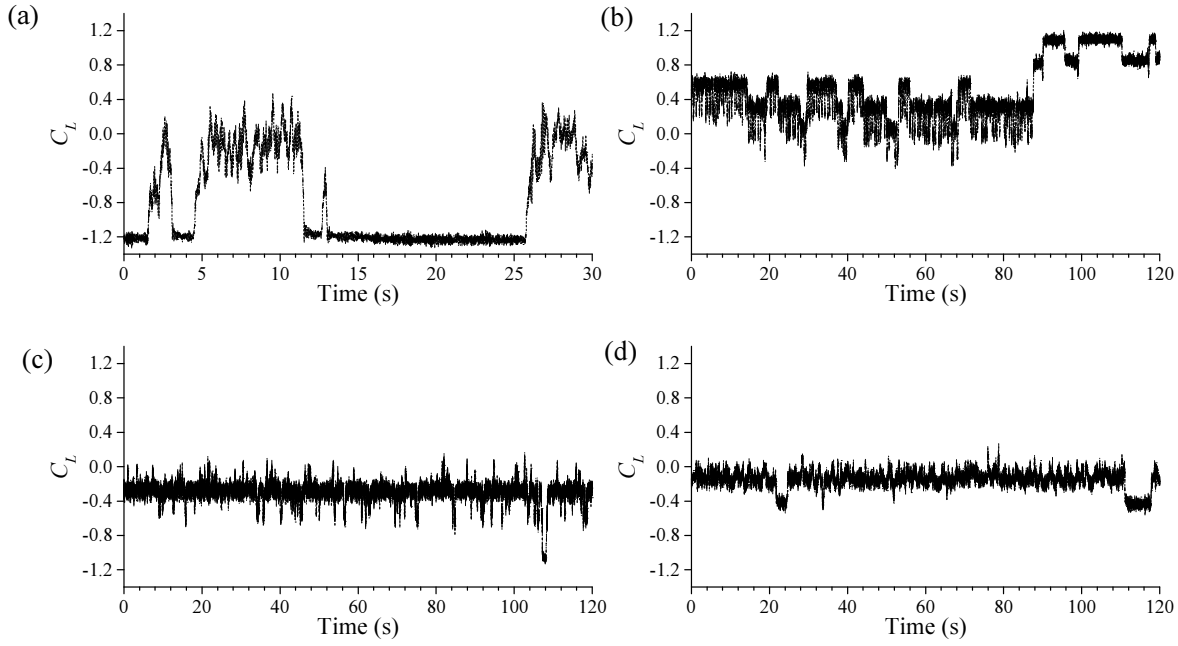

Fig. 9 Jumps in lift coefficients at various surface roughness values for (a). Smooth, Re=3.81×10^5, (b) K/D=0.002%, Re=3.67×10^5, (c) K/D=0.005%, Re=3.71×10^5, and (d) K/D=0.009%, Re=3.67×10^5.

To summarize, the surface roughness influences the following aspects of aerodynamic forces and flow states for a circular cylinder in the critical Reynolds number regime.

(1) Rough surfaces reduce the occurrence of transition at lower Reynolds number.

(2) Rough surface reduces the significance of the "drag crisis" process, in the range of Reynolds number it covers and reduces the drop in C_D. from the maximum (subcritical) to a minimum. This means that rough surfaces induce more efficient transition.

(3) The non-zero mean lift coefficients decrease for rougher cylinders and finally disappear because of the reduction in strength of the single separation bubble (TrBL1) with increasing surface roughness.

(4) Over the critical Reynolds number range, the lift coefficient fluctuations are primarily due to low-frequency components induced by separation and reattachment instead of vortex shedding which is dominant in the subcritical regime. This phenomenon is changed by the influence of surface roughness on the boundary layer.

(5) Jumps in lift coefficients in time, corresponding to different flow states in TrBL0-1, become weaker and then disappear as the surface roughness increases.

4. Responses of the elastically mounted cylinder

4.1 Effects of surface roughness on average displacements

In the static tests, the variation of lift coefficients represents the transition in the boundary layer process with the mean being zero in TrBL0, non-zero in TrBL1 and close to zero in TrBL2. This process was also observed in the dynamic tests through the change of average vertical displacement. Two tests, designated the first and the second, were performed with an arbitrary rotation to the cylinders to confirm the response for each elastically mounted model. The mean normalized displacement D_v/D, as shown in Fig. 13, indicates that the mean lift with non-zero values corresponds to the TrBL1 regime. Similar to the static tests (Fig. 3), two tests for the elastically mounted cylinders show good consistency in the trends. The maximum of the mean D_v/D decreases with increasing surface roughness.

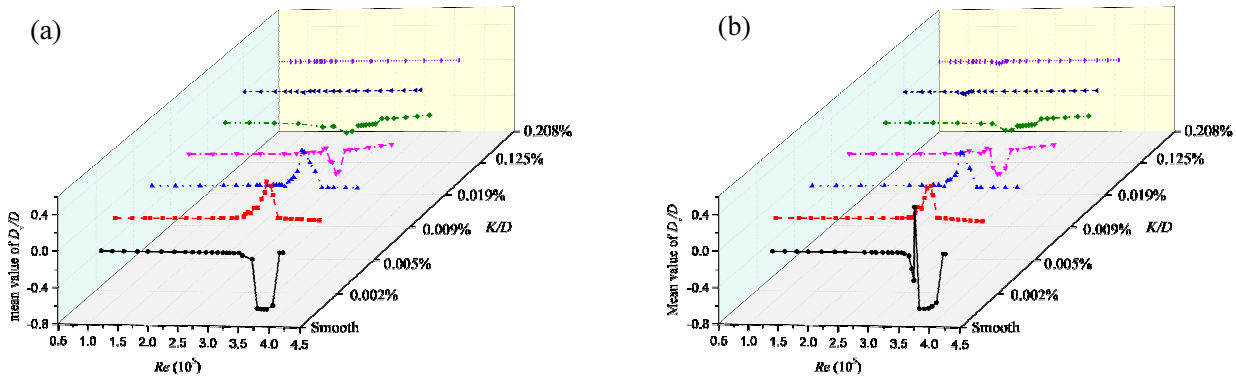

Fig. 10 Variation of mean normalized vertical displacement with *Re* at various *K/D* for (a) the first test, and (b) the second test.

Aerodynamic forces on the cylinders in the dynamic tests can be estimated through the measured displacement and stiffness of the elastically mounted system which includes four springs at each end. Fig. 11 (a) compares the maximum absolute values of the lift coefficients, $|C_L|_{max}$, and the corresponding Reynolds numbers for the three static tests and two dynamic tests. For all tests with the flow state in TrBL1, the onset of the $|C_L|_{max}$ is in the TrBL1 regime. The value of $|C_L|_{max}$ reflects the strength of the separation bubble. Generally, all five tests show a good agreement in $|C_L|_{max}$. The static and dynamic tests show insignificant differences in $|C_L|_{max}$ at various surface roughness cylinders. As shown in Fig. 11 (b), large differences in the corresponding Reynolds numbers are shown at K/D= 0.125% and 0.208% for the first dynamic tests in which the TrBL1 does not occur, and the mean lift coefficients are approximately zero. For the cases showing TrBL1 states ($K/D \leq 0.019\%$ in the present study), the corresponding Reynolds numbers show a good agreement in trends for static and dynamic tests. It seems that the difference between the Reynolds numbers for the static and dynamic tests becomes larger for the rougher cylinders. Therefore, the transition may occur at a lower Reynolds number for elastically mounted cylinders than for stationary cylinders.

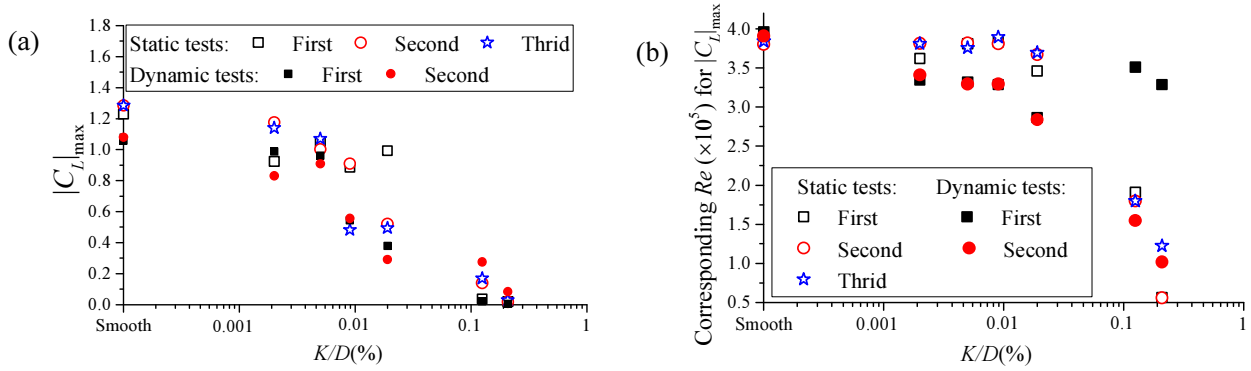

Fig. 11 Comparison of lift coefficients for the static tests and dynamic tests in (a) $|C_L|_{max}$ and (b) the corresponding *Re* for $|C_L|_{max}$.

4.2 Vibrations in the critical Reynolds number range

Dry galloping has been observed in the critical Reynolds number range in several wind tunnel tests(Cheng et al, 2008a; Cheng et al, 2008b; Jakobsen et al, 2012; Nikitas and Macdonald, 2015). In the present study, vibrations in the critical Reynolds number range are observed for the smooth and rough cylinders, but the onset of the vibrations is not in the entire range of the critical Reynolds number. As an example, Fig. 12 shows the variation of the vibrations with the Reynolds number for the smooth cylinder in the first dynamic test. The mean and Std of D_y/D is shown in Fig. 12 (a). The non-zero mean vertical displacements reflect the formation of a separation bubble on one side of the cylinder and present the flow in the TrBL1 regimes. Five cases of four flow regimes are chosen. Fig. 12 (a), for the smooth cylinder, shows that the largest vibrations occur at 3.73×10^5 which correspond to TrBL0-1 at which there is a change in the mean D_y/D from zero

(TrBL0) to a non-zero value (TrBL1). There is also an increase in the standard deviation of D_v/D at Re=4.06×10^5 which corresponds to TrBL1-2, which is evident because it occurs as the mean D_v/D goes from the non-zero value (TrBL1) back to zero (TrBL2). To illustrate the difference between vibrations in TrBL0-1, TrBL1, TrBL1-2, and TrBL2, vibrations at Re=3.57×10^5, 3.73×10^5, 3.96×10^5, 4.06×10^5 and 4.17×10^5 are shown in Fig. 12 (b), (c), (d), (e) and (f) respectively. The amplitude at 4.06×10^5 in TrBL1-2 is larger than that in TrBL1 and TrBL2. This vibration corresponds to the formation of a second separation bubble. Unlike the vibrations in TrBL0-1, jumps in the mean D_v/D are not observed in TrBL1-2. This difference can be attributed to the different formation processes of the two separation bubbles. When a transition occurs in the boundary layer on one side of the cylinder and the flow reattaches at the rear of the cylinder, the final separation point on the bubble side is farther leeward than on the non-bubble side. The formation of the first separation bubble makes the flow asymmetrical. When the second separation bubble forms, the transition occurs in the boundary layer on the other side of the cylinder and makes the flow symmetric again. It is easier to induce the symmetrical flow state for a circular cylinder in the uniform flow. As shown in Fig. 12 (a), TrBL0-1 is across a wider Reynolds number range than TrBL1-2.

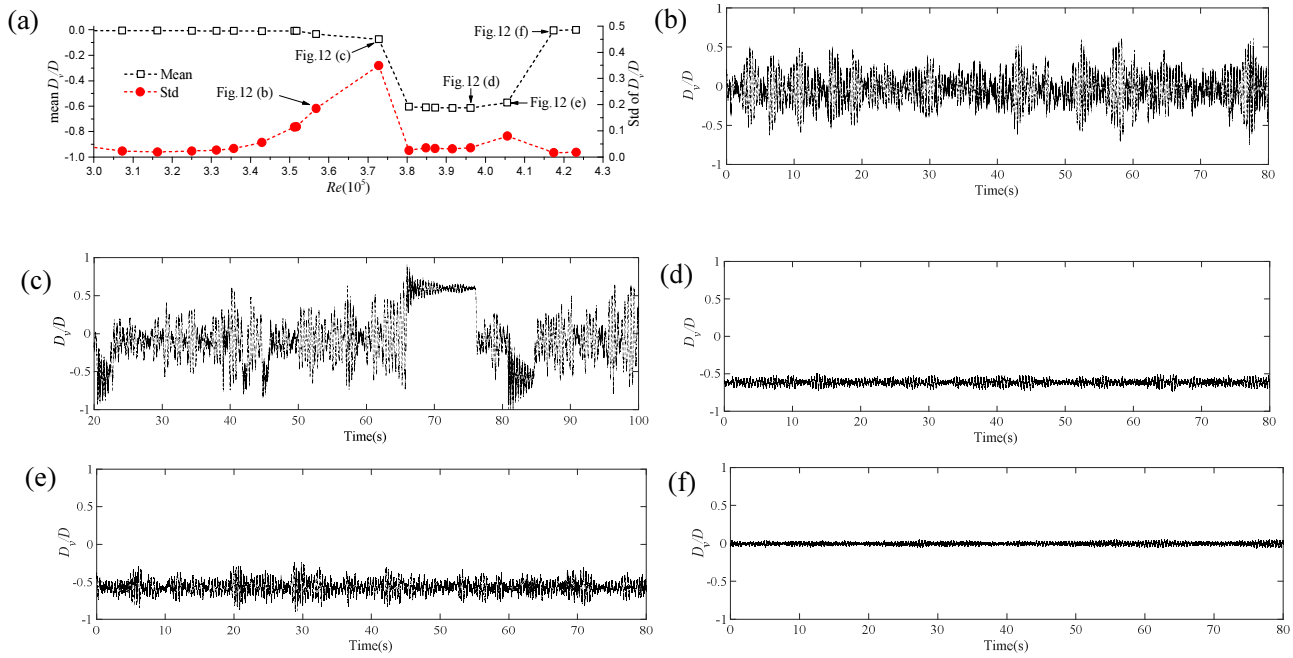

Fig. 12 Vibrations for the smooth cylinder: (a) mean and standard deviation of D_v/D in the critical Reynolds number range, (b) Re=3.57×10^5, in TrBL0-1, (c) Re=3.73×10^5, in TrBL0-1, (d) Re=3.96×10^5, in TrBL1, (e) Re=4.06×10^5, in TrBL1-2, and (f) Re=4.17×10^5, in TrBL2

Based on the results in Fig. 12, the smooth cylinder vibrates when the flow changes from one state to another in the critical Reynolds number range. There are two types of vibration that are observed in TrBL0-1 and TrBL1-2, respectively. The largest amplitude vibrations are more likely to occur in TrBL0-1. The jumps in these vibrations show that the flow state changes from non-reattachment to reattachment. The amplitudes in TrBL1-2 are much smaller than that in TrBL0-1.

4.3 Effects of surface roughness on the vibrations

To evaluate the effects of surface roughness on the vibrations, the maximum standard deviation of D_v/D for each surface roughness and the corresponding Reynolds numbers are shown in Fig. 13. The standard deviations are based on the whole sampling period. Large amplitude vibrations in the present study are simply defined as those vibrations in which the maximum standard deviation of D_v/D exceeds 0.1. Similar to the vibrations for the smooth cylinder, the

maximum standard deviation of D_v/D for the rough cylinders is observed in TrBL0-1, for which there are large vibrations.

Based on this definition of large amplitude vibrations, the large amplitude vibration occurs for the less rough cylinders with a surface roughness of up to 0.009%. As shown in Fig. 13, in general, the maximum standard deviation of D_v/D decreases with increasing surface roughness. The maximum standard deviations of vertical displacement for the cylinders with K/D=0.019%, 0.125%, and 0.208% are less than 0.03. The corresponding Reynolds number drops dramatically between K/D=0.019% and 0.125%. It seems that the vibrations for the larger values of roughness are related to vortex shedding. In Fig. 6, St is reidentified through the spectrum of lift coefficients in the critical Reynolds number range when K/D= 0.125% and 0.208%. This implies that a sufficiently rough surface can also mitigate the Reynolds number related vibrations.

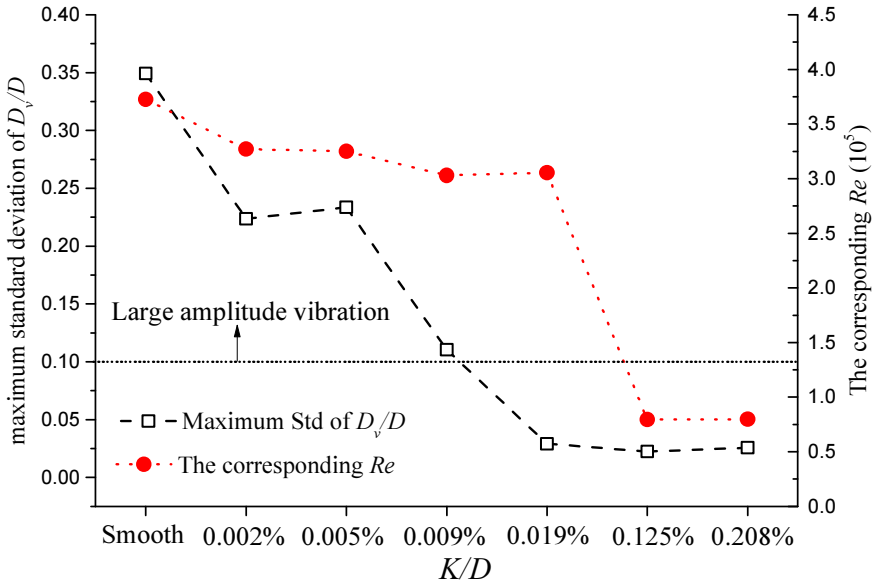

Fig. 13 Variation of the maximum standard deviation of D_v/D and the corresponding Re with surface roughness.

Time histories of the normalized vertical displacement for the maximum amplitude vibrations for each surface roughness are shown in Fig. 14. To illustrate the frequency change in the energy distribution with time, Fig. 14 also shows continuous wavelet transform coefficients of each series by using the complex Morlet wavelets. The colors in Fig. 14 indicated by the color bar represent the value of wavelet transform coefficient. The time histories for K/D=0.019%, 0.125% and 0.208% are included to illustrate that the vibrations were insignificant. The difference in amplitude with surface roughness reveals the same trend as that shown by the standard deviation in Fig. 13. All the observed large vibrations are unsteady in amplitude. Two features are worth discussing. First, similar to the jumps in static lift coefficients (Fig. 9), Fig. 14 shows jump in the vertical displacements at approximately 70 s and 82 s in Fig. 14 (a), at 150 s and 178 s in Fig. 14 (b), and at 25 s in Fig. 14 (c). These jumps provide further evidence that the large amplitude vibrations occur in the TrBL0-1 transition. The magnitude of the jump decreases as the surface roughness increases until no significant jumps are evident for K/D=0.009% (Fig. 14 (d)). Second, the amplitude of the vibrations when the mean displacement is non-zero is smaller than when the mean displacement is close to zero, as seen at approximately 70s in Fig. 14 (a) and in 150s in Fig. 14 (b), respectively. Additionally, the vibrations around the non-zero means tend to decay in amplitude, in a manner typical of free vibrations. This is clear near 70 s in Fig. 14 (a) and 150 s in Fig. 14 (b) and appears to occur near 21 s and 82 s in Fig. 14 (a). This implies that when a stable separation bubble has formed, although there is a non-zero mean lift force, there is little dynamic forcing. This is consistent with Fig. 9 (a), in which the lift fluctuations near zero are significant but in the state with mean C_L=1.2, the lift fluctuations are negligible.

Similar to the effect of surface roughness on vibrations in TrBL0-1, surface roughness promotes the occurrence of

transition sufficiently in TrBL1-2. Furthermore, it reduces the amplitude of the vibrations because it shortens and weakens the TrBL1-2 transition process. In the present study, the significant vibrations in TrBL1-2 are only observed for the cylinder with a smooth surface and K/D=0.002%,0.005%, and 0.009%. Their amplitudes are small (standard deviation of D_v/D less than 0.1) and differ insignificantly..

Several features can be obtained through the wavelet maps. Please note that fD/U is from 0 to 0.1 in Fig. 14 (a)-(e) because the energy in the range of fD/U=0.1-0.5 is ignorable in these cases. First, for the large amplitude vibrations (Fig. 14 (a)-(d)), the energy concentrated at fD/U <0.01 approximately corresponds to the natural frequency when the cylinder vibrates. The vortex shedding frequencies in fD/U=0.1-0.5 for the TrSL, TrBL1, and TrBL2 flow regimes are not identified. This means that these vibrations are due to the low-frequency components as shown in Fig. 7. However, the coupling mechanism of low-frequency components in a lift with the vibration remains unclear. Second, the wavelet maps also show a discontinuity in the strength. This confirms the unsteadiness of the large amplitude vibrations. Third, as shown Fig. 14 (f), the wavelet map shows a clear main contribution from the vortex shedding in fD/U=0.21-0.23. This contribution reflects the fact that the motion in this case is a forced vibration that is excited by the vortex induced forces. The vibration in this case is different from dry galloping or Reynolds number related vibrations.

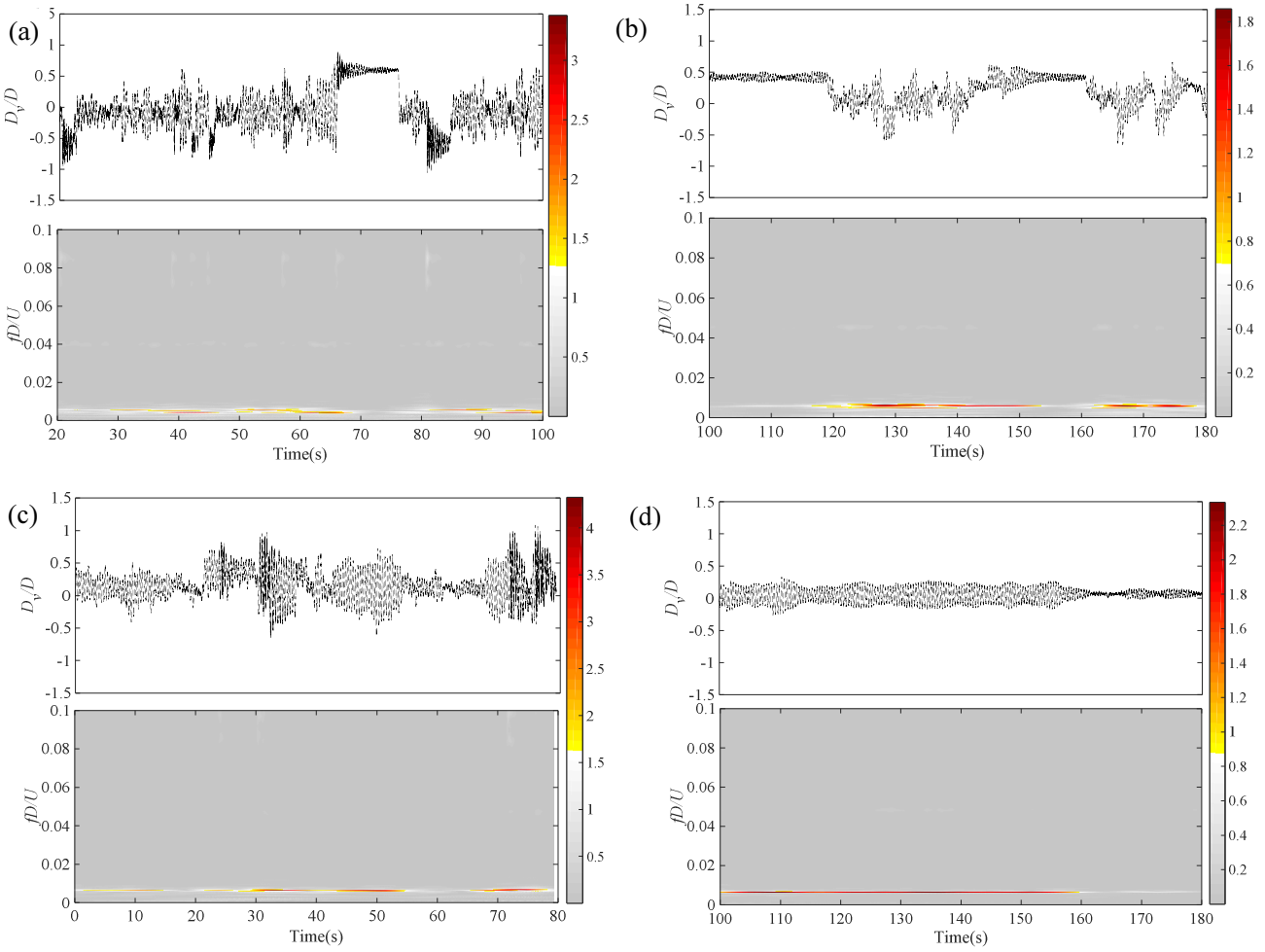

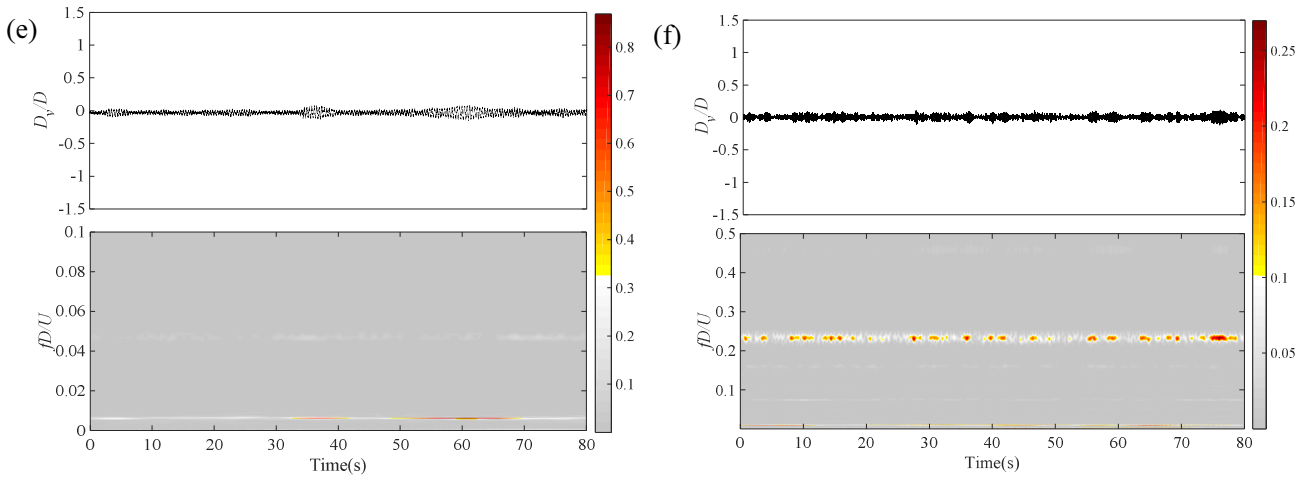

Fig. 14 Time histories for the maximum amplitude vibration for each cylinder: (a) Smooth, Re=3.73×10^5 (b) K/D=0.002%, Re=3.27×10^5 (c) K/D=0.005%, Re=3.25×10^5 (d) K/D=0.009%, Re=3.08×10^5 (e) K/D=0.019%, Re=3.15×10^5 (f) K/D=0.125%, Re=2.03×10^5

It is clear that surface roughness can reduce the amplitude of the vibrations in the critical Reynolds number range. This trend agrees well with the effect of surface roughness on the aerodynamic forces on circular cylinders in the critical Reynolds number range.

5. Conclusions

The effects of surface roughness on the aerodynamic forces on a circular cylinder are investigated in more details. The results show that the surface roughness significantly reduces the features of aerodynamics in the critical Reynolds number range. These influences probably can be attributed to the increases in skin friction and roughness-generated turbulence.

The onsets of Reynolds number related vibrations observed in the present study show that the vibrations strongly depend on the transition between two flow regimes rather than the entire critical Reynolds number range, mostly between TrBL0 and TrBL1. The unsteadiness of the vibrations implies a bistable flow state when the cylinders vibrate. Surface roughness reduces the Reynolds number related vibrations by making a sufficient transition. In other words, the process of transition occurs in narrower Reynolds number range for the rougher cylinder. The bistable states are mitigated by sufficient surface roughness. This mitigation suppresses the Reynolds number related vibrations. In the present study, the relative surface roughness ranges in value across three orders of magnitude: hundred thousandth, ten thousandth, and thousandth. Reynolds number related vibrations are not observed for cylinders the when relative surface roughness is approximately on the order of thousandth. Therefore, Reynolds number related vibrations are less likely to occur for a rough cylinder in reality.

Acknowledgments

The authors gratefully acknowledge the support of the National Natural Science Foundation of China (Grant No. 51778381), Natural Science Foundation of Hebei Province (Grant No. E2017210107 and ZD2018063), Collaborative Innovation Centre of Preventing Disasters and Reducing Damages for Large Infrastructures in Hebei Province and the China Scholarship Council for Wenyong Ma's visit to the University of Bristol.

References

Achenbach, E., 1971. Influence of surface roughness on the cross-flow around a circular cylinder. J Fluid Mech 46, 321-335.

Achenbach, E., 1981. On vortex shedding from smooth and rough cylinders in the range of Reynolds number 6×103 to 5×106. J Fluid Mech 109, 239-251.

Bearman, P.W., 1969. On vortex shedding from a circular cylinder in the critical Reynolds number region. J Fluid Mech 37, 577-587.

Benidir, A., Flamand, O., Gaillet, L., Dimitriadis, G., 2015. Impact of roughness and circularity-defect on bridge cables stability. Journal of Wind Engineering and Industrial Aerodynamics 137, 1-13.

Cheng, S., Irwin, P.A., Tanaka, H., 2008a. Experimental study on the wind-induced vibration of a dry inclined cable Part II: Proposed mechanisms. Journal of Wind Engineering and Industrial Aerodynamics 96, 2254-2272.

Cheng, S., Larose, G.L., Savage, M.G., Tanaka, H., Irwin, P.A., 2008b. Experimental study on the wind-induced vibration of a dry inclined cable Part I: Phenomena. Journal of Wind Engineering and Industrial Aerodynamics 96, 2231-2253.

Eisner, F., 1925. Druckmessungen an umströmten Zylindern. ZeZeitschrift für angewandte Mathematik und Mechanik 5-6, 486-489.

Jakobsen, J.B., Andersen, T.L., Macdonald, J.H.G., Nikitas, N., Larose, G.L., Savage, M.G., McAuliffe, B.R., 2012. Wind-induced response and excitation characteristics of an inclined cable model in the critical Reynolds number range. Journal of Wind Engineering and Industrial Aerodynamics 110, 100-112.

MA, W., LIU, Q., DU, X., LIU, X., 2017a. Aerodynamic forces and galloping instability for a skewed elliptical cylinder in a flow at the critical Reynolds number. Fluid Dynamics Research 49, 045509.

Ma, W., Macdonald, J.H.G., Liu, Q., 2017b. Aerodynamic characteristics and excitation mechanisms of the galloping of an elliptical cylinder in the critical Reynolds number range. Journal of Wind Engineering and Industrial Aerodynamics 171, 342-352.

Ma, W., Macdonald, J.H.G., Liu, Q., Nguyen, C.H., Liu, X., 2017c. Galloping of an elliptical cylinder at critical Reynolds number and its quasi-steady prediction. Journal of wind engineering and industrial aerodynamic 168, 110-122.

Matsumoto, M., Ishizaki, H., 2017. Rain and Wind Induced Vibration and Dry Galloping of Stay Cables -Its Mechanism and Aerodynamic Stabilization.

Matsumoto, M., Yagi, T., Hatsuda, H., Shima, T., Tanaka, M., Naito, H., 2010. Dry galloping characteristics and its mechanism of inclined/yawed cables. Journal of Wind Engineering and Industrial Aerodynamics 98, 317-327.

Matteoni, G., Georgakis, C.T., 2015. Effects of surface roughness and cross-sectional distortion on the wind-induced response of bridge cables in dry conditions. Journal of Wind Engineering and Industrial Aerodynamics 136, 89-100.

Nikitas, N., Macdonald, J.H.G., 2015. Aerodynamic Forcing Characteristics of Dry Cable Galloping at Critical Reynolds Number. European Journal of Mechanics - B/Fluids 49, 243-249.

Nikitas, N., Macdonald, J.H.G., Jakobsen, J.B., Andersen, T.L., 2012. Critical Reynolds number and galloping instabilities: experiments on circular cylinders. Exp Fluids 52, 1295-1306.

Schewe, G., 1983. On the force fluctuations acting on a circular in crossflow from subcritical up to transcritical Reynolds numbers. J Fluid Mech 133, 265-285.

Schewe, G., 1986. Sensitivity of transition phenomena to small perturbations in flow around a circular cylinder. J Fluid Mech 172, 33-46.

Zdravkovich, M.M., 1997a. Flow Around Circular Cylinders Vol 1: Fundamentals. Oxford University Press, New York.

Zdravkovich, M.M., 1997b. Flow Around Circular Cylinders Vol 2: Applications. Oxford University Press, New York.